Forecasting Research

Met O 11 Scientific Note No. 8

An analytical model of the growth of a frontal intrusion

by

M. Holt and G.J. Shutts

November 1988

Meteorological Office (Met O 11)
Bracknell, Berkshire RG12 2SZ, England

An analytical model of the growth of a frontal intrusion

by

M. W. Holt and G. J. Shutts

Meteorological Office, London Road, Bracknell RG12 2SZ England

LONDON, METEOROLOGICAL OFFICE.
Met.O.11 Scientific Note No.8

An analytical model of the growth of a frontal intrusion.

00371288 551.515.81 FH2A

November 1988

Abstract

An analytic semi-geostrophic model of frontogenesis is described which exhibits the growth of a frontal discontinuity surface of finite length . The initial distribution of temperature on a plane horizontal boundary consists of a warm two-dimensional strip embedded in an isothermal background. The potential vorticity is uniform and positive. A barotropic deformation field with axis of dilation along the warm strip forces a vertical front with velocity discontinuity as the warm air is occluded and detaches from the lower boundary.

The solution demonstrates some important general properties of the inviscid semi-geostrophic equations when discontinuities are present . In particular the vertical velocity at the lower boundary is zero everywhere except at the front where it becomes ill-defined. At the time when the front first forms the vertical velocity has a maximum at the point discontinuity . Also the front itself constitutes a line source of potential vorticity so that the global integral of mass-weighted potential vorticity is only conserved if the boundary of the domain is redefined in such a way as to exclude the front. Both properties have practical implications for numerical modelling.

For typical atmospheric rates of deformation forcing the accelerations of air parcels close to the front are sufficiently large to violate the conditions of validity of semi-geostrophic theory but not those for hydrostatic balance.

1. Introduction

Gill (1981) showed how exact balanced states of rectilinear flow on an f-plane may be obtained by a conformal mapping technique , and found a class of flow states which represent homogeneous intrusions in a stratified medium of uniform potential vorticity. Solutions containing discontinuities of finite length were found by Shutts (1987) and Purser and Cullen (1987) : they were considered to be rudimentary models of atmospheric fronts. The solutions found by Shutts (1987) were considered to represent the balanced flow resulting from the instantaneous removal of an infinite tube of fluid, with elliptical cross-section, oriented parallel to the direction of the flow. Ou (1983) considered the geostrophic adjustment of an incompressible fluid initially at rest but with vertical isopycnals - a system with zero potential vorticity. When the curvature of the density profile (in the horizontal coordinate) exceeded a critical value, Ou noted that fluid initially in contact with the upper and lower boundaries must detach and move into the interior of the fluid along a frontal surface if a solution is to be found . This separation process actually creates a front as particles with different values of density and absolute momentum are brought together. A similar problem was solved by Cullen (1983) in the context of frontogenesis under the action of a deformation flow. A general technique for constructing finite element approximations to balanced rectilinear flow states with embedded discontinuities was outlined by Cullen and Purser (1984). They argued that the inviscid semi-geostrophic equations could in principle be solved whether or not discontinuities were present and that the frontogenesis problem considered by Hoskins and Bretherton (1972) could be continued beyond the point when a discontinuity first

forms. They also suggested that the geostrophic separation process accompanying the formation of fronts would be associated with the intrusion of a line source of potential vorticity - an apparent violation of the requirement that the global-mean mass-weighted potential vorticity be conserved (Haynes and McIntyre, 1987).

The physical relevance of the discontinuity predicted by inviscid semi-geostrophic theory may be questioned for at least two reasons : firstly the scaling assumptions on which the equations are based will break down in some region about the developing front ; and secondly mixing will smooth out the velocity and temperature contrast across the front. For the purpose of comparison with the atmosphere we assume, consistent with observations, that the frontal discontinuity will be limited to a thickness over which the local Richardson number is about 1/4 . Gall et al (1987) have shown, using a very high resolution two-dimensional model, that a front collapses to the horizontal grid scale even when this is as small as 280 m. Many aspects of the Gall simulation support the concept of a growing frontal discontinuity proposed by Cullen and Purser (1984) in spite of the failure of the balance assumption near the front. The analytic model to be presented here is used to illustrate some of the properties noted above and to assess the likely range of validity of the semi-geostrophic assumption.

Our interest centres on steady rectilinear flows on an f-plane , which have vertical and cross-stream variation of flow speed . To be steady such flows must be in geostrophic and hydrostatic balance and therefore satisfy the thermal wind relation . A Cartesian coordinate system is adopted with x , y , z representing the cross-stream , along

stream and vertical coordinates respectively. The flow is assumed to occupy the upper half space $z > 0$ with z taken as the pseudo-height coordinate of Hoskins and Bretherton (1972). The state of balance can then be expressed as :

$$fv_g = \partial\varphi/\partial x \qquad (1)$$

$$g\theta/\theta_o = \partial\varphi/\partial z \qquad (2)$$

where v_g is the y-component of the geostrophic wind , θ is the potential temperature with reference value θ_o , φ is the geopotential , f is the Coriolis parameter and g is the acceleration due to gravity (f, g and θ_o are assumed constant). Following Gill (1981) we introduce a characteristic height scale H, time scale f^{-1} and buoyancy frequency N ; and define a horizontal length scale NH/f , a velocity scale NH , a potential temperature scale $N^2H\theta_o/g$ and a geopotential scale $(NH)^2$. These are used to non-dimensionalise the relevant equations so that eqns. (1) and (2) become :

$$v_g = \partial\varphi/\partial x \qquad (3)$$

$$\theta = \partial\varphi/\partial z \qquad (4) \ .$$

Introducing the absolute momentum $M = x + v_g$ and letting the non-dimensional potential vorticity have unit value then equations (3) and (4) imply ,

$$\partial M/\partial z = \partial \varphi/\partial x \qquad (5)$$

and we have from the definition of potential vorticity ,

$$\partial(M, \theta)/\partial(x, z) = 1 \qquad (6) \quad .$$

Finally, following Gill (1981), eqs. (5) and (6) may be written as the Cauchy-Riemann equations :

$$\partial\theta/\partial M = - \partial x/\partial Z \qquad (7)$$

$$\partial\theta/\partial Z = \partial x/\partial M \qquad (8)$$

where Z is the same coordinate as z but differentiation is with M held constant (ie. M and Z are treated as independent variables).

Eqs. (7) and (8) imply a general conformal mapping

$$x + i\theta = F(M + iZ)$$

where F() represents any analytic function.

The conformal mappings dealt with in this paper associate all particles in the x-z plane , $z > 0$ with the region in M-θ space indicated in Fig. 1 - that is, the upper half plane of M-θ except for an elliptical indentation centred on the origin. We show that the horizontal discontinuity map described by Shutts (1987) arises as the limit of a particular conformal mapping , and that a family of solutions including an upright discontinuity, a point discontinuity and an unperturbed atmosphere at rest may be generated by varying a parameter in the

mapping. A sequence of solutions corresponding to the continuous deformation of an elliptical indentation of the lower boundary of the domain in M-θ coordinates is also constructed. Different descriptions of the mapping are required for different ranges of eccentricity of the ellipse. The cases where the major axis of the ellipse is vertical correspond to a line discontinuity in absolute momentum at $x = 0$. It is shown how points on the indentation of the boundary in M-θ space map onto points bounding this frontal discontinuity , leading to the identification of the front with the locus of points initially on $z = 0$ (for the ellipses of aspect ratio < 1) that are forced away from $z = 0$ (for the ellipses of aspect ratio > 1). Because these solutions have the same horizontally stratified flow at infinity, any two members of the family may be related by a time t and a deformation parameter in such a way that we may consider one solution to have arisen from the other under the action of deformation.

2. The Conformal Mapping solutions

(a) Mapping 1

If we take the mapping used by Gill (1981) and Shutts (1987) to describe an elliptical lens of homogeneous fluid, and interchange x and M with θ and z respectively, the region corresponding to the half-lens $\theta > 0$ in x-z of their solution becomes an elliptical indentation in the lower boundary of the region in M-θ coordinates.

The general form of the mapping is then:

$$Y = a \cosh[\sinh^{-1}\{W \cosh(\alpha_o)\} - \alpha_o] \qquad (9)$$

where

$$W = x + i\theta \qquad (10)$$

$$Y = M + iZ \qquad (11)$$

and a and α_o are constants .

Using the parametric coordinates (α, β) as in Gill (1981) we define

$$\zeta = \alpha + i\beta \qquad (12)$$

$$Y = M + iZ = a \cosh(\zeta - \alpha_o) \qquad (13)$$

$$W = x + i\theta = \operatorname{sech}(\alpha_o)\sinh(\zeta) \qquad (14)$$

for $\alpha \geq 0$, $0 \leq \beta \leq \pi$.

The requirement $W \to Y$ as $|Y| \to \infty$ (for a horizontally stratified atmosphere at rest a long way from the origin) gives

$$a = 1 + \tanh(\alpha_o). \qquad (15)$$

The lower boundary of the region in M-θ space ($\alpha = \alpha_o$) is then given by :

$$M^2/a^2 + \theta^2 = 1 \quad |M| < a \qquad (16)$$

$$\theta = 0 \quad |M| > a .$$

For $\alpha_o \geq 0$ we have $1 \leq a \leq 2$ so the indentation varies from a semicircle to a half-ellipse of eccentricity 1/2 with major axis along $\theta = 0$. Cross-sections of M and θ for this solution for the values $\alpha_o = 10$ and $\alpha_o = 0$ are shown in Figs. 2. In Appendix 1, it is shown that the limit $\alpha_o \to \infty$ of this map corresponds to the horizontal discontinuity map of Shutts (1987) . There is a singularity in the solution at the ends of this discontinuity (at x = +/- 1 in Figs 2a and 2b). As α_o decreases the width of the warm strip shortens until at $\alpha_o = 0$ the singularities merge at the origin (Figs. 2c and 2d).

To extend this solution to allow $0 \leq a \leq 1$ requires $\alpha_o < 0$ which causes the map from (α, β) to (x, z) to become multivalued for some $\alpha < 0$. This may be avoided by taking only that part of the α-β plane with

$$\alpha > 0 \qquad 0 < \beta < \pi \quad \text{for } \alpha_o < 0$$

$$\alpha \geq \alpha_o \qquad 0 < \beta < \pi \quad \text{for } \alpha_o \geq 0 \ .$$

This would allow us to construct the solution where the ellipse in the M-θ lower boundary has its major axis vertical, which is the requirement for the map to contain a front. However if we consider how the variables behave on the ellipse boundary we find that for $\alpha_o < 0$ the boundary is given by $\alpha = 0$, and that as $\alpha_o \to -\infty$ the indentation vanishes. As will be discussed further in Section 3, this is inconsistent with the effect of frontal deformation which causes the elliptical indentation to contract along the M-axis but leaves the height of the ellipse unchanged. The following mapping avoids this problem.

(b) Mapping 2

In order to construct a sequence of solutions where the potential temperature at the top of the front remains constant ($\theta = 1$) as the front develops, it is necessary to modify Map 1 so that the ellipse has its major axis in the θ direction.

A mapping with the required properties is given by

$$\theta + ix = W' = \cosh\left[\sinh^{-1}\{Y'\cosh(\alpha_o)\} - \alpha_o\right] \tag{17}$$

$$z + iM = Y' = \sinh(\zeta)/(a\cosh(\alpha_o))$$

where as before

$$a = 1 + \tanh(\alpha_o)$$

and the primes on W and Y distinguish these complex variables from those in §2a .

This is effectively a transformation and rescaling of the ellipse generated by the first mapping. It is readily shown that $W' \sim Y'$ for large $|W'|$ and $|Y'|$. The lower boundary of the M-θ domain is now given by $\alpha = \alpha_o$ and for $\alpha_o \geq 0$ we can obtain the elliptical indentation up to eccentricity 1/2, with major axis along $M = 0$. The height of the front , given by the value of z at the top of the ellipse , ranges from 0 to 1/2 as α_o goes from 0 to ∞.

In parametric coordinates

$$\theta = \mathrm{Cosh}(\alpha-\alpha_o)\mathrm{Cos}\ \beta$$

$$x = \mathrm{Sinh}(\alpha-\alpha_o)\mathrm{Sin}\ \beta$$

and the top of the front corresponds to $(\alpha_o, 0)$ in the α-β plane , at which point $\theta = 1$.

(c) Mapping 3

To continue the range of solutions the same transformation and rescaling are applied to the ' thin lens ' mapping of Gill (1981) , giving the third mapping :

$$a = 1 + \coth(\alpha_o) \qquad \alpha_o \geq 0$$

$$\theta + ix = W' = \cosh(\zeta - \alpha_o) \tag{18}$$

$$z + iM = Y' = \cosh(\zeta)/(a \sinh(\alpha_o)) \quad .$$

Cross-sections of M and θ for different choices of α_o with mappings 2 and 3 are shown in Figs. 3 and 4. Here as $\alpha_o \to 0$ in mapping 3 the height of the front tends to 1, but the strength of the front as measured by the jump in M across $x = 0$ tends to zero, since it can be shown that : $[M] = 2/a = 2/(1 + \coth(\alpha_o))$, and $\coth(\alpha_o) \to \infty$. Thus as we see in Fig. 3(e) and 4(e) for small α_o the frontal perturbation vanishes and we are left with the background horizontally stratified atmosphere at rest. This corresponds to the application of an infinite amount of deformation to the initial state of Fig. 2(a) , as described in the next section .

A summary of the parametric representation of the mappings used is given in Appendix 2.

3. The related frontogenesis problem

Each solution given by the conformal mappings of the previous section is an exact, time-independent flow state with convective and symmetric stability . However we may also consider the solutions to be be part of a sequence arising through the action of a barotropic deformation flow. It has long been accepted (see e.g. the review paper of Hoskins (1982)) that the simplest dynamical mechanism for frontogenesis is the pure deformation flow , given by :

$$u_g = - \alpha_D x$$

$$v_g = + \alpha_D y \ . \qquad (19)$$

Any pre-existing horizontal temperature gradient in the x - direction will become concentrated under its influence. For our two-dimensional study, we consider the cross-section in the plane y = 0 . Hoskins and Bretherton (1972) showed, using semi-geostrophic theory, that such a flow is able to produce a discontinuity in a finite time .

For this flow we have :

$$DM/Dt = - \alpha_D M$$

$$D\theta/Dt = 0 \, . \qquad (20)$$

Individual fluid parcels must therefore obey the equation:

$$M = M_o \exp(-\alpha_D t) \qquad (21)$$

so that M and θ are known for all time in terms of their initial values.

Applying this to the conformal mapping solutions we may take the initial state to be that shown in Fig. 2 (a) and (b). Then any other state may be related to this by a time t given by (see Fig. 5):

$$M_2 = M_1 \exp(-\alpha_D t)$$

that is

$$\alpha_D t = \ln(M_1/M_2) \qquad (22)$$

where M_1 and M_2 are the initial and final (time t) half-widths of the ellipse.

For an initial state that does not contain a front the value of M at the base of the ellipse ($\alpha = \alpha_o$, $\beta = 0$) is given by

$$M(t) = a(t) = 1 + \tanh[\alpha_o(t)] \qquad (23)$$

so we see that the front will form when a = 1 ($\alpha_o = 0$); that is in a time τ given by:

$$\alpha_o \tau = \ln[1 + \tanh\{\alpha_o(0)\}] \quad (24).$$

As we move to map 2 , α_o increases from 0 to ∞ as the front grows to height 1/2 , then moving into map 3 α_o decreases from ∞ to 0 as $t \to \infty$. The variation of α_o with time as we move through the 3 mappings is shown in fig 6 . In practice the largest value of α_o used is that for which $\tanh(\alpha_o) \approx 1$.

By looking at the corresponding time dependence of the parametric coordinates α, β and α_o for a fluid parcel, instantaneous values of the vertical and horizontal velocities and accelerations may be diagnosed in accordance with eq. (20). We have x, z, M and θ given as functions of α, β and α_o for a particular fluid parcel and so differentiating and applying the chain rule we obtain Dx/Dt , Dz/Dt , DM/Dt and $D\theta/Dt$ as functions of α, β, α_o, $D\alpha/Dt$, $D\beta/Dt$ and $D\alpha_o/Dt$.

Air parcels initially on the elliptical indentation will remain there and conserve their values of M_o and θ , thus for the point at the base of the ellipse in the first mapping we have from eqs. (22) and (23) :

$$1 + \tanh(\alpha_o(t)) = [1 + \tanh(\alpha_o(0)]\exp(-\alpha_o t) \quad (25).$$

So by differentiating this expression with respect to time we obtain an expression relating $D\alpha_o/Dt$ to α_o .

Eqs. (20) may now be written as:

$$0 = D\theta/Dt = F_1(\alpha, \beta, \alpha_o, D\alpha/Dt, D\beta/Dt)$$

$$-\alpha_o M = DM/Dt = F_2(\alpha, \beta, \alpha_o, D\alpha/Dt, D\beta/Dt) \quad (26)$$

where F_1 and F_2 are known functions. These two equations may be solved for $D\alpha/Dt$ and $D\beta/Dt$ at each point (α , β) thereby allowing Dx/Dt and Dz/Dt to be evaluated from D/Dt (eq. 17). The same process may be applied to the eqs. (26) to obtain expressions for $D^2\alpha/Dt^2$ and $D^2\beta/Dt^2$ allowing Du/Dt and Dw/Dt to be evaluated .

Cross-sections of the vertical velocity calculated by this method are shown in Figs. 7. If α_0^{-1} is equivalent to one day in dimensional units then Fig. 7 (a) corresponds to a time 15 hours before the appearance of the discontinuity. A broad zone of ascent is indicated on the scale of the warm air strip on the surface. As the forcing proceeds a low-level maximum in vertical velocity appears ; Fig. 7(b) shows the cross section some 2½ hours before the front forms. The position of maximum updraught speed descends until the maximum is located at the surface at the point of singularity at the time the front forms (Fig 7(c)) . After the front has formed the vertical velocity maximum rises from the surface , coincident with the top of the front , and the circulation weakens. (Figs 7(d) and 6(e))

The implication that w is non-zero at the ground when $t = \tau$ deserves some closer inspection. A fluid particle at the tip of the front has $\alpha = \alpha_0$ and $\beta = 0$ which, from mapping 2, has a height $z_F = a^{-1}\mathrm{Tanh}(\alpha_0)$. But by a similar argument to that leading to eq. (25) it can be shown that:

$$\alpha_0(t-\tau) = \ln[1+\mathrm{Tanh}\ \alpha_0] = \ln(a) \qquad (27)$$

so that:

$$z_F = 1-\exp[-\alpha_D(t-\tau)]. \qquad t \geq \tau \qquad (28)$$

The vertical velocity at the top of the front is therefore given by:

$$\frac{dz_F}{dt} = \alpha_D \exp[-\alpha_D(t-\tau)] \qquad (29)$$

which demands that

$$\frac{dz_F}{dt} = \alpha_D \quad , \quad z_F=0 \quad \text{at time } \tau.$$

A time series of vertical velocity for an air parcel which finds itself near the top of the front is shown in Fig 8.

Considering the evolution of the ageostrophic circulation as the frontogenesis takes place, we know by symmetry that both u and u_{ag} are zero on x = 0 . For points on the warm strip at the surface (on the indentation $\alpha = \alpha_0$) we have $u_{ag} = -\alpha_D\cos(\beta)$, so that u_{ag} is a maximum at the endpoints of the warm strip [$\beta = \pi/2$, $x = +/-(a-1)$] . Since conservation of θ for fluid on the indentation implies conservation of coordinate β following a fluid parcel , so u_{ag} is conserved for these fluid parcels . Thus as the forcing proceeds the two endpoints of the warm strip move towards the origin , retaining the values of u_{ag} . Therefore between these two points $\partial u_{ag}/\partial x$ increases , so from symmetry and continuity $\partial w/\partial z$ on the line x = 0 also increases . This continues until at $t = \tau$ the two points are coincident at the origin , forming the singularity . Both $\partial u_{ag}/\partial x$ and $\partial w/\partial z$ are infinite at the origin , as the maximum in vertical velocity reaches the surface .

The instant the front forms there is an infinite acceleration bringing the flow u_{sg} to rest at x = 0 . The region close to the front around the x - axis also experiences a rapid deceleration of the flow . It can be shown that as we move to map 2 the acceleration along the x - axis has a term proportional to 1/x near the origin at time τ . From figures (not shown) $\partial u_{sg}/\partial x$ near the front appears uniform with height below the top of the front , and so therefore is $\partial w/\partial z$. With w = 0 at the surface the maximum vertical velocity is located at the top of the growing front. As the forcing proceeds the ageostrophic circulation weakens , until as $t \to \infty$ we return to the basic state atmosphere at rest .

4. Validity of the hydrostatic and semi-geostrophic approximations

The condition for the semi-geostrophic approximation to be valid is that $D\underline{v}/Dt$ should be much smaller than $f\underline{v}$. Hoskins (1975) expressed this in intrinsic coordinates which in non-dimensional form gives two scalar inequalities :

$$|V^{-1}DV/Dt| \ll 1 \qquad (25a)$$

$$|D\chi/Dt| \ll 1 \qquad (25b)$$

where V is the magnitude of the horizontal component of velocity and χ is the angle made between the horizontal projection of the velocity and a fixed reference line . The semi-geostrophic equations are valid therefore if both the streamwise acceleration and the rate of turning of

the horizontal wind are small . With the Boussinesq approximation, the vertical component of the non-dimensional momentum equation becomes:

$$f^2/N^2 \, Dw/Dt \quad + \partial\varphi'/\partial z = \theta' \quad (26)$$

We may define $\theta' = \theta - z$ as the perturbation from the uniformly stratified background atmosphere and compare this term with calculated values of $f^2/N^2 Dw/Dt$. The hydrostatic assumption is valid provided that the ratio $|f^2/N^2 Dw/Dt \, /\theta'|$ is much smaller than 1. This is always found to be the case and the ratio is of order 10 $f^2/N^2 \approx 10^{-3}$ at maximum . The acceleration and rate of wind turning ratios (on the left of the inequalities 25 (a)and (b)) at , just before and just after the time of formation of the front are shown in Fig. (9) .

Before formation of the front the breakdown occurs over a 'candle flame' shaped region above the origin . Taking a height scale H of 1km the region extends to a height of some 40m above the origin and maximum width of the order of 1km. With the dimensional value of α_D^{-1} approximately 1 day the ratios first exceed 0.3 some 30 minutes before the front forms . These values agree with the recent findings of Davies and Müller (1988) , who found that , for a different surface potential temperature profile , the semi-geostrophic approximation broke down some 30 minutes before the formation of the front , and over a region some 30m high by 1km wide . The flow modelled in this paper is directly comparable with the 'symmetric' solution presented by Davies and Müller (1988) , but the conformal method of solution allows the frontogenesis to proceed beyond the time of formation of the discontinuity , allowing the front to grow into the domain . Time series for a fluid parcel which

finds itself above the growing front are shown in figure 10 a and b , and we see that after the front forms the accelerations become small for this parcel . However, as was described in the discussion of the ageostrophic circulation , on formation of the discontinuity there is a deceleration of the u component , proportional to 1/x, which eventually brings the ageostrophic flow to rest . This causes the acceleration and rate of turn ratios to exceed 0.3 in a 'half flame' shaped region in each direction along the x-axis (fig 9d,e) for a short time immediately after formation of the front , while at the same time the accelerations in the region above the front have moderated . Thus the region in which the semigeostrophic approximation breaks down before the front forms is totally separate from the region in which the breakdown occurs after the front has formed. A time-series of the ratio term for a parcel which passes through this region is shown in fig 10c .

Physically , if the region of breakdown acts as a source of gravity waves during the frontal collapse , in this model the source would be switched off instantaneously and switched on in another location at the time the front forms . Because of the small time and length scales involved only a very small part of the gravity wave spectrum will be excited . If we consider the flow toward the origin along the x-axis ; before the front forms the air coasts in towards the origin without hindrance , the continuity equation being satisfied by an increasing ascent above the origin , but once the front has formed the flow effectively sees a 'brick wall' at the origin , hence the dramatic deceleration and breakdown of the semigeostrophic criteria along the x-axis .

5. Discussion and Conclusions

We have presented an exact solution representing the growth of a vertical front consistent with the semi-geostrophic equations. Although from a physical viewpoint the model is rather contrived, it does have the virtue of displaying a number of important properties of inviscid frontogenesis taken beyond the point of discontinuity onset at the boundary. The solution has implications not only for our physical understanding and numerical modelling of front formation but also for the interpretation of potential vorticity diagnostics as the following discussion shows.

Cullen and Purser (1984) argue that inviscid frontogenesis involves the formation of discontinuity lines (ie. 'true' fronts) intruding into the interior of a fluid in semi-geostrophic balance. They also propose that these frontal discontinuities appear as line sources of potential vorticity (PV). Their growth would seem at first sight to be inconsistent with ideas recently re-emphasised by Haynes and McIntyre (1987) - that the mass-weighted volume integral of PV should be a constant in the absence of boundary fluxes. The domain-averaged PV will increase as the fronts grow if we do not redefine the position of the boundary. If, however, the front itself is regarded as part of the boundary so that the boundary contour follows but does not intersect the front, then the domain-averaged PV is constant.

In order to understand this frontal contribution to the global PV consider the lower boundary in M-θ and x-z spaces corresponding to the vertical front in Fig.3 (b) as depicted in Figs. 11 . The thick solid line in Fig. 11 (a) represents the 'ground' in physical space with the front marked by a zig-zag line. The dashed line in Fig. 11 (a) is

the boundary contour referred to above which does not cut the front. The associated contours in M-θ space are similarly depicted in Fig. 11 (b).

Here the mass-weighted volume integral of PV is given by

$$\int_D q \, dxdz = \int_{D'} dMd\theta$$

where D is any region in physical space corresponding to D' in M-θ space. Clearly the volume-integrated PV obtained using the solid-line boundary will be greater than that obtained using the dashed line by an amount equal to the area of the shaded half-ellipse. By allowing the front to be part of the interior fluid we have admitted the shaded region of M-θ space even though it maps to a line of zero volume in physical space (implying infinite PV).

If we allow the fluid to have finite viscosity for a very small though finite time period, the front would become blurred over a finite horizontal length scale and fluid particles could be found for all (M, θ) values in the shaded region. In other words, very high PV values would be found over the small finite fluid volume affected by the diffusion. Real fronts should therefore be identifiable as zones of very high PV since turbulent mixing will also prevent the formation of a true discontinuity. Diabatic heating in real fronts also tends to create a low-level PV maximum and so it is important to be able to distinguish between these separate contributions. Numerical simulations of dry frontogenesis by Keyser and Anthes (1982) clearly show sources of PV at the base of their model frontal zone which they found to be due to heat and momentum sources created by boundary layer mixing. We suggest that this PV source is not an accident of the form of boundary layer

parametrization but is the inevitable consequence of the smoothing of the frontal discontinuity at the smallest resolvable scale.

The frontal discontinuity line is certain to be unstable at the smallest scales of motion but may also be unstable at horizontal length scales of the order of the Rossby deformation radius based on the height of the front. This is likely since a necessary condition for instability in a two-dimensional flow (the generalised Charney-Stern criterion - see Eliassen, 1983) is that the potential vorticity should have a maximum on some isentropic surfaces. This is true of those surfaces which pass through the front in our idealised model

Another interesting implication of this analytical study is the high degree of imbalance near the incipient front. Gravity wave activity is likely to be greatest at the time of appearance of the boundary discontinuity. The vertical velocity maximum descends rapidly as this time approaches until - in the solution - it touches the ground as the boundary front forms. Thereafter, the flow settles down again with the imbalance confined to a shrinking region near the base of the front (fig. 8d) . Note that if the deformation was at any time switched off, the fluid would adjust to the semi-geostrophic solution at that time *provided that no irreversible physical processes had occurred earlier* (eg. gravity wave breaking)

Of some modelling significance is the fact that the warm fluid initially in contact with the ground has been lifted clean away from the surface after the discontinuity has formed so that $\theta=0$ on $z=0$. On the other hand the usual material boundary condition $w=0$ at $z=0$ implies in practical terms that fluid in the lowest model layer will tend to remain there - irrespective of the separation effect predicted by the

solution. The use of high vertical resolution in the boundary layers of current operational weather forecasting models probably does much to alleviate this difficulty , by allowing diffusive transfer away from a very shallow surface layer .

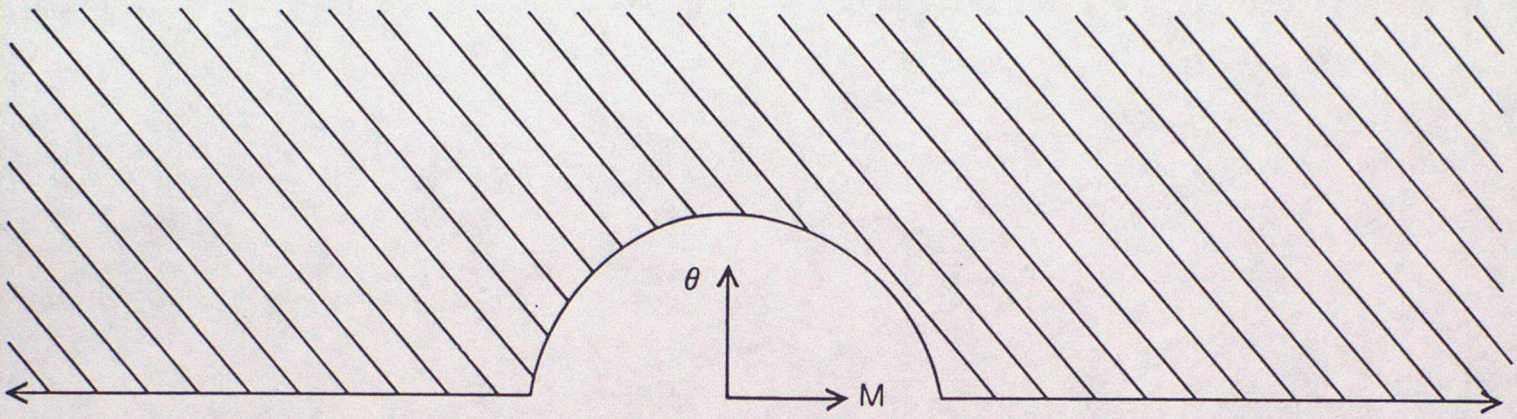

figure 1

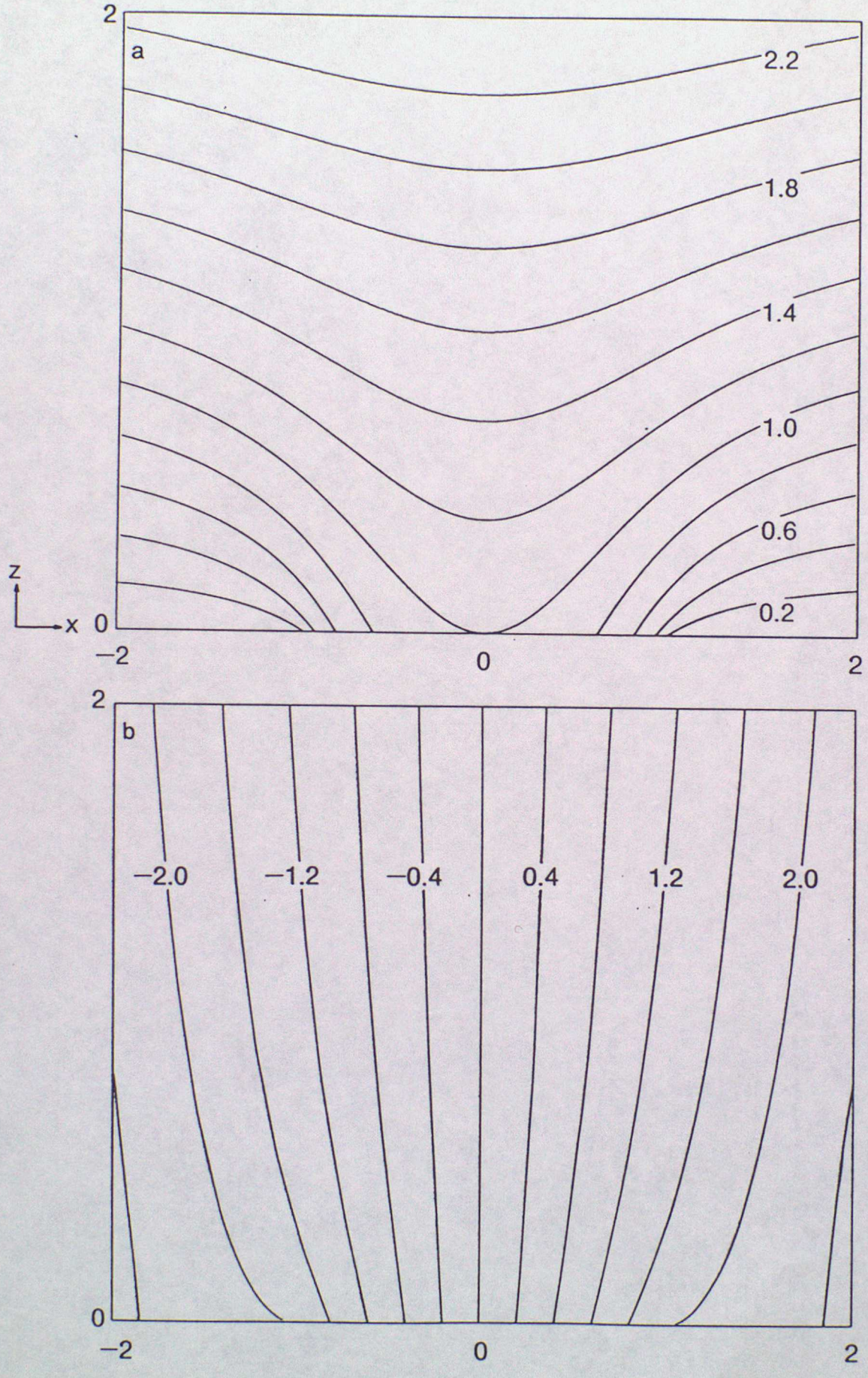

figure 2 (a) θ 2(b) M for map 1 with α_o = 10.

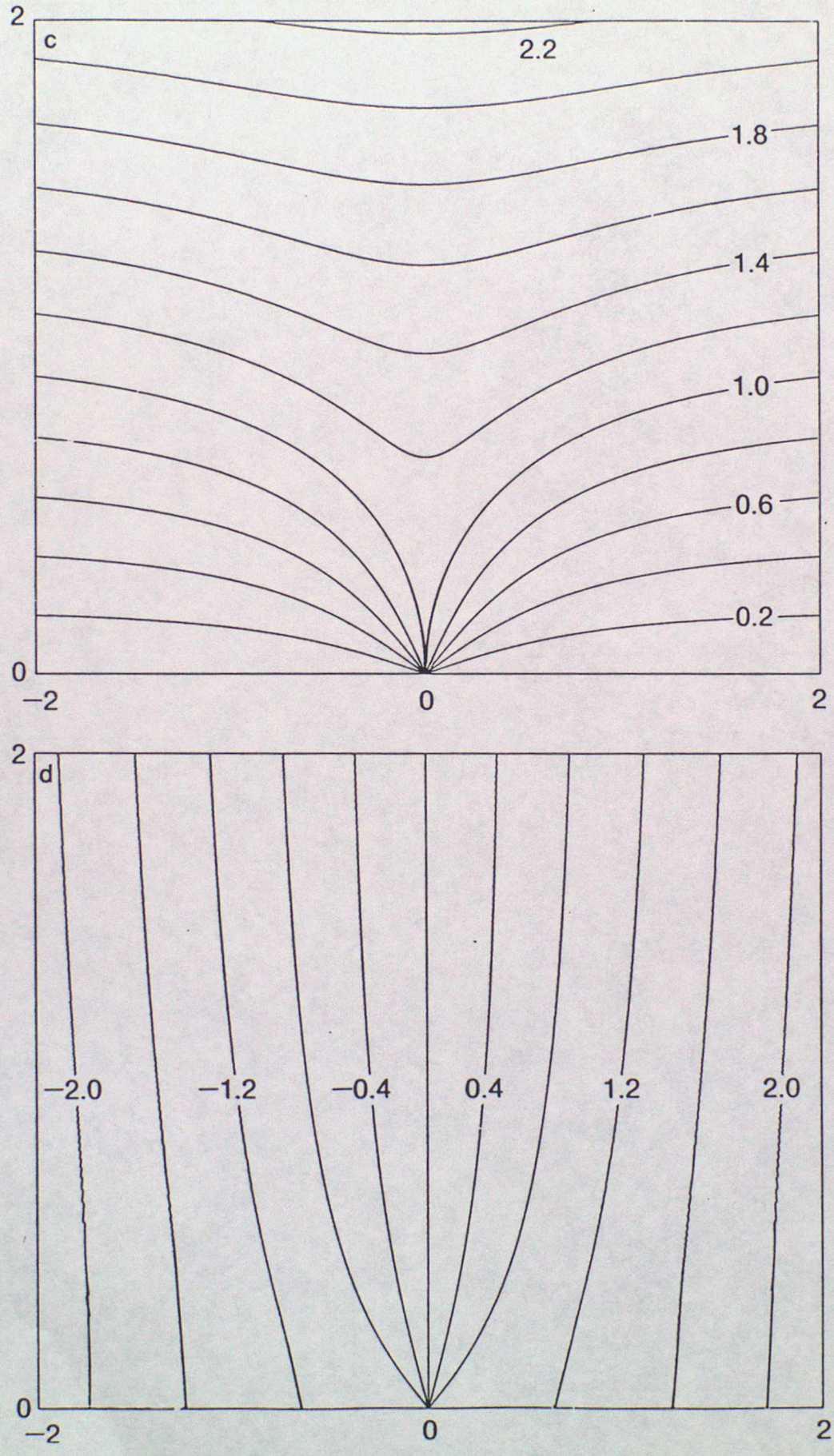

figure 2 (c) θ and (d) M for map 1 with $\alpha_o = 0$

at the time of onset of the singularity at the origin .

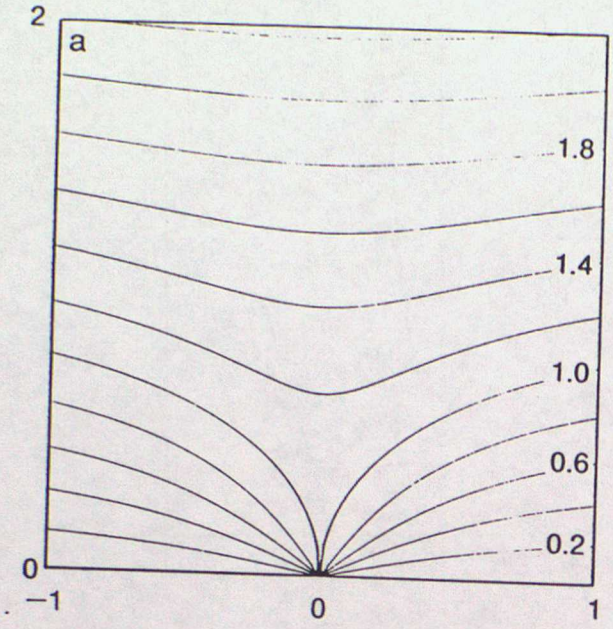

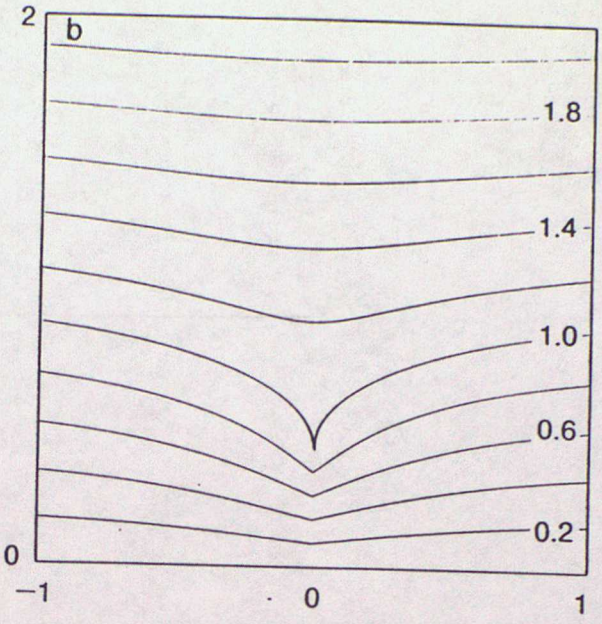

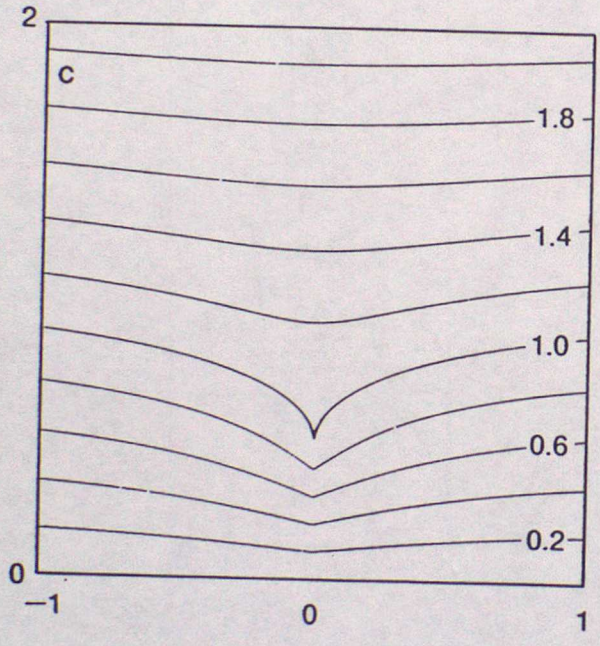

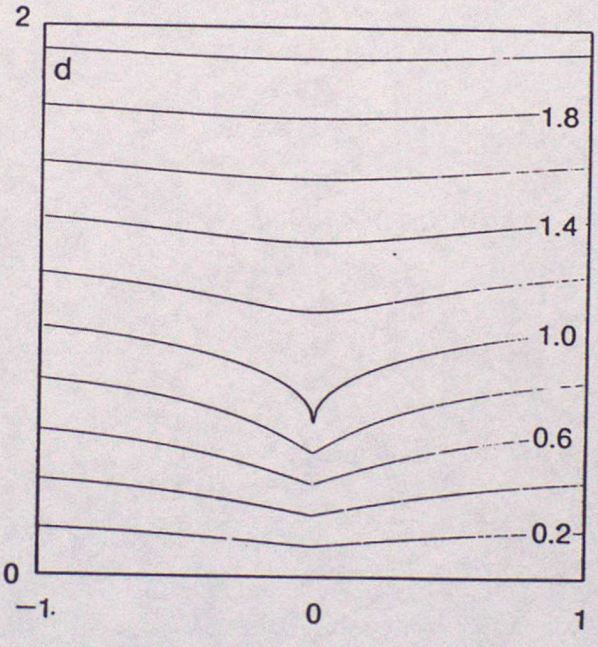

figure 3 Cross sections of θ :

(a) map 2 α_o = 0

(b) map 2 α_o = 1

(c) map 2 α_o = 10

(d) map 3 α_o = 1

(e) map 3 α_o = 0.1

showing how the perturbation vanishes in the limit.

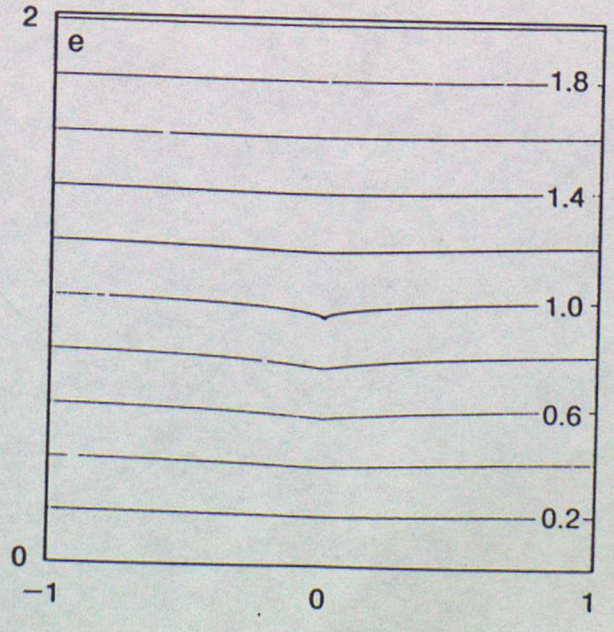

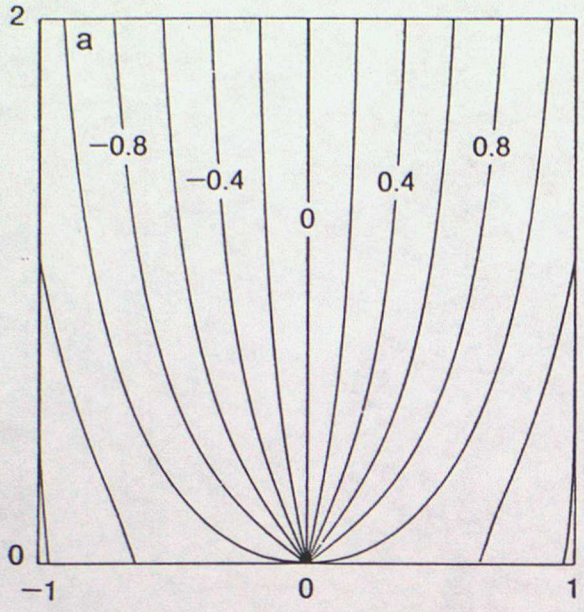

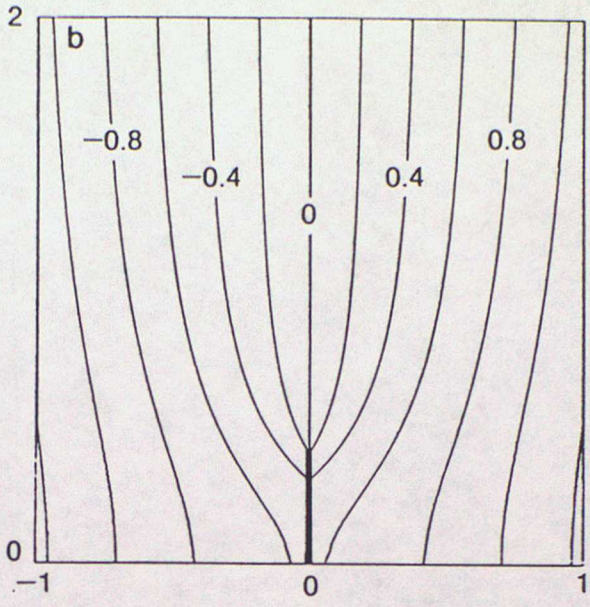

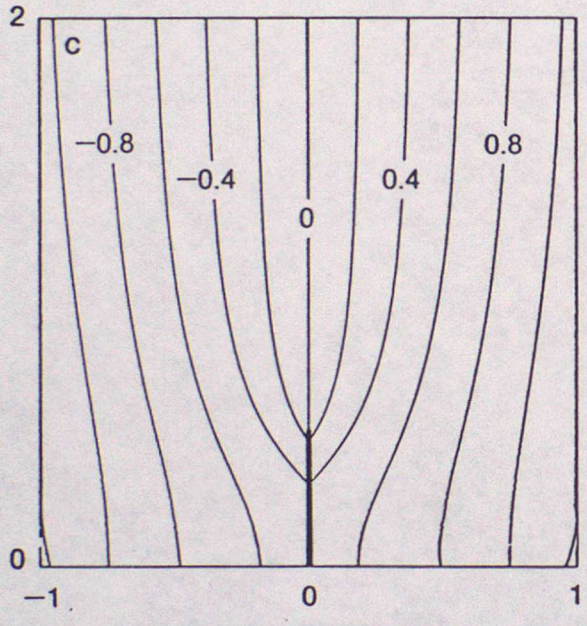

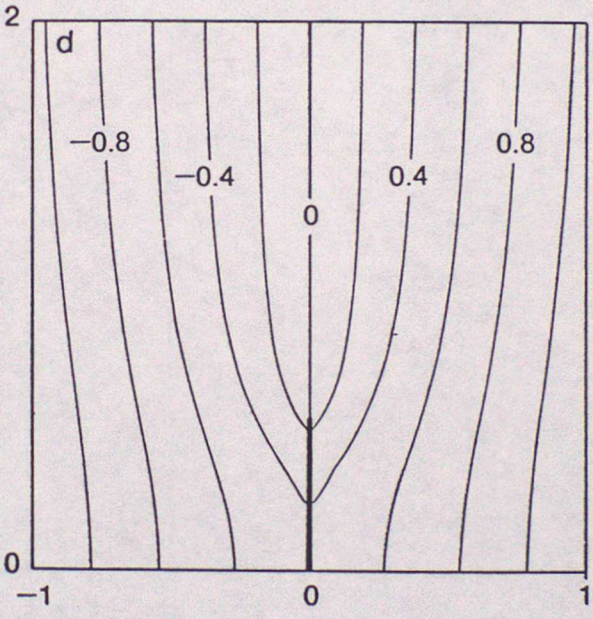

figure 4 Cross sections of M, as in figure 3.

The discontinuity in M has been marked with a thick black line.

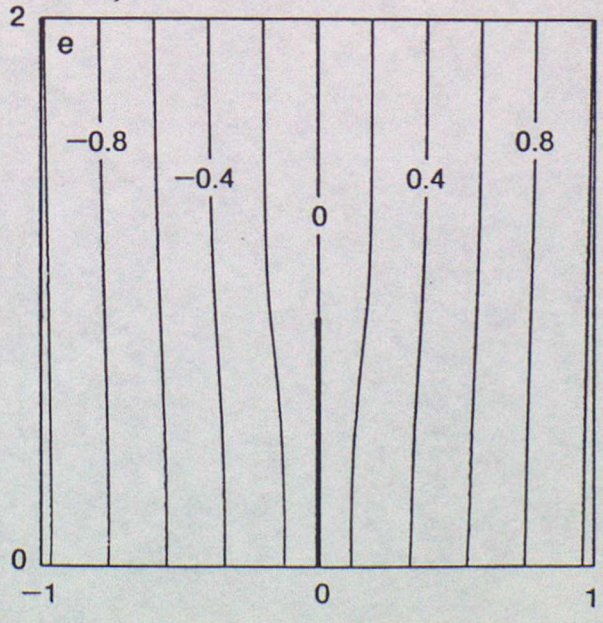

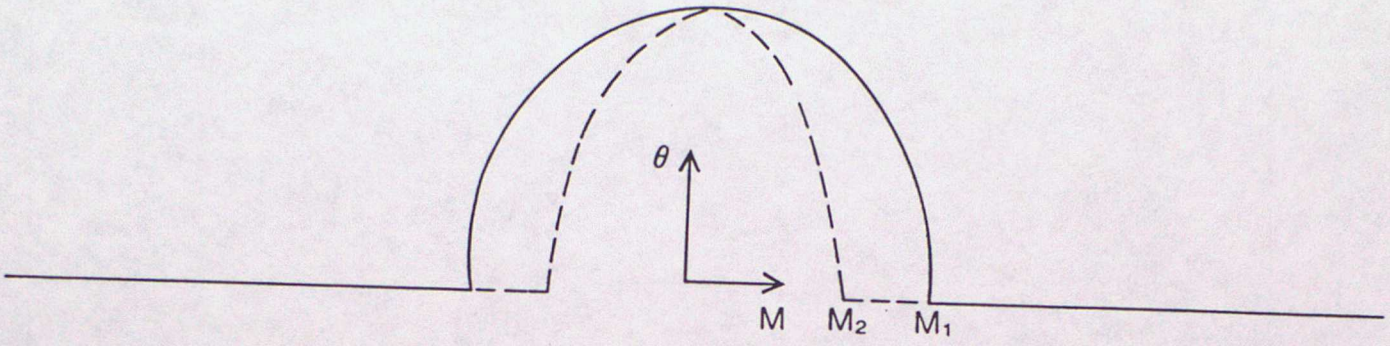

figure 5

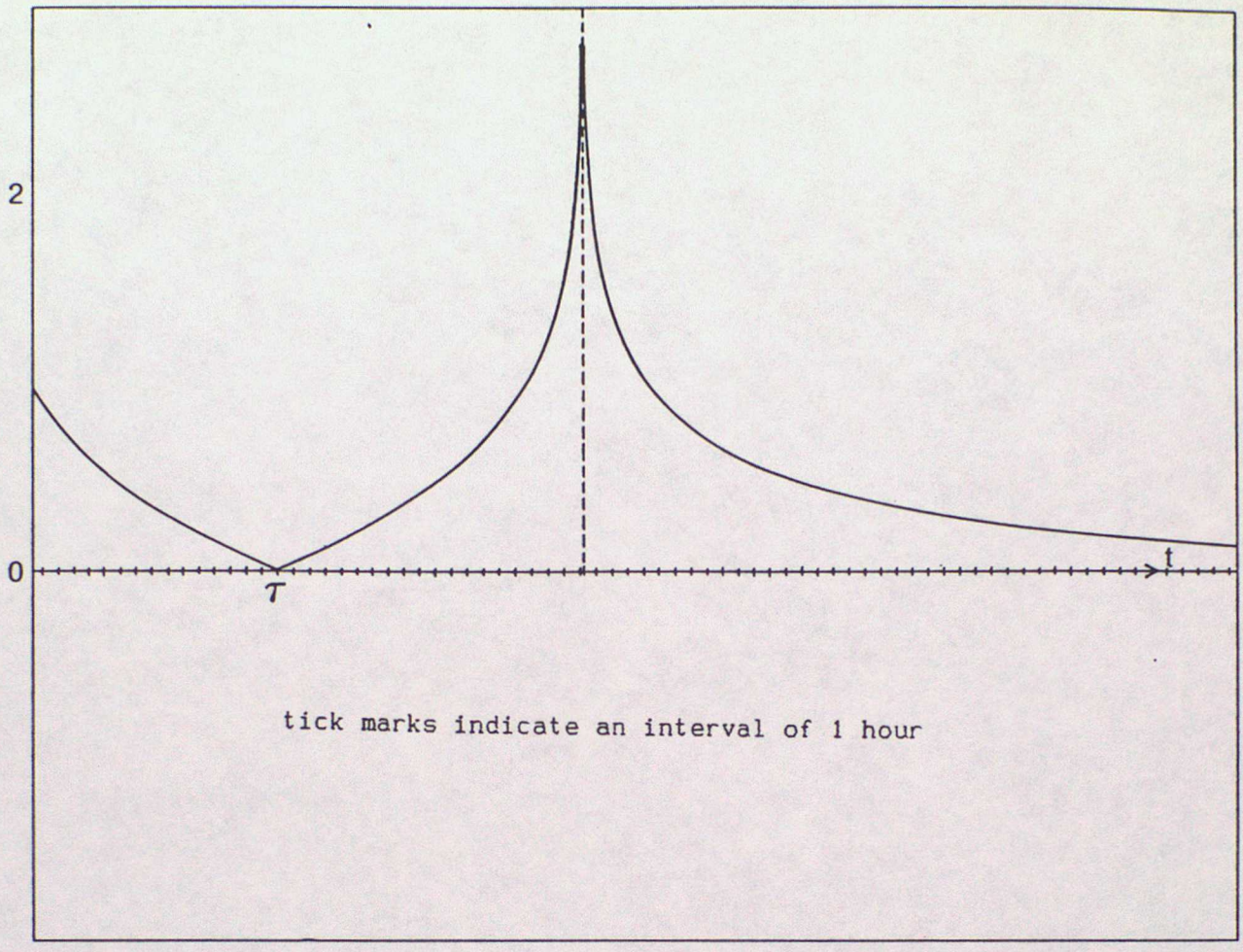

figure 6 Showing how α_o varies with time.

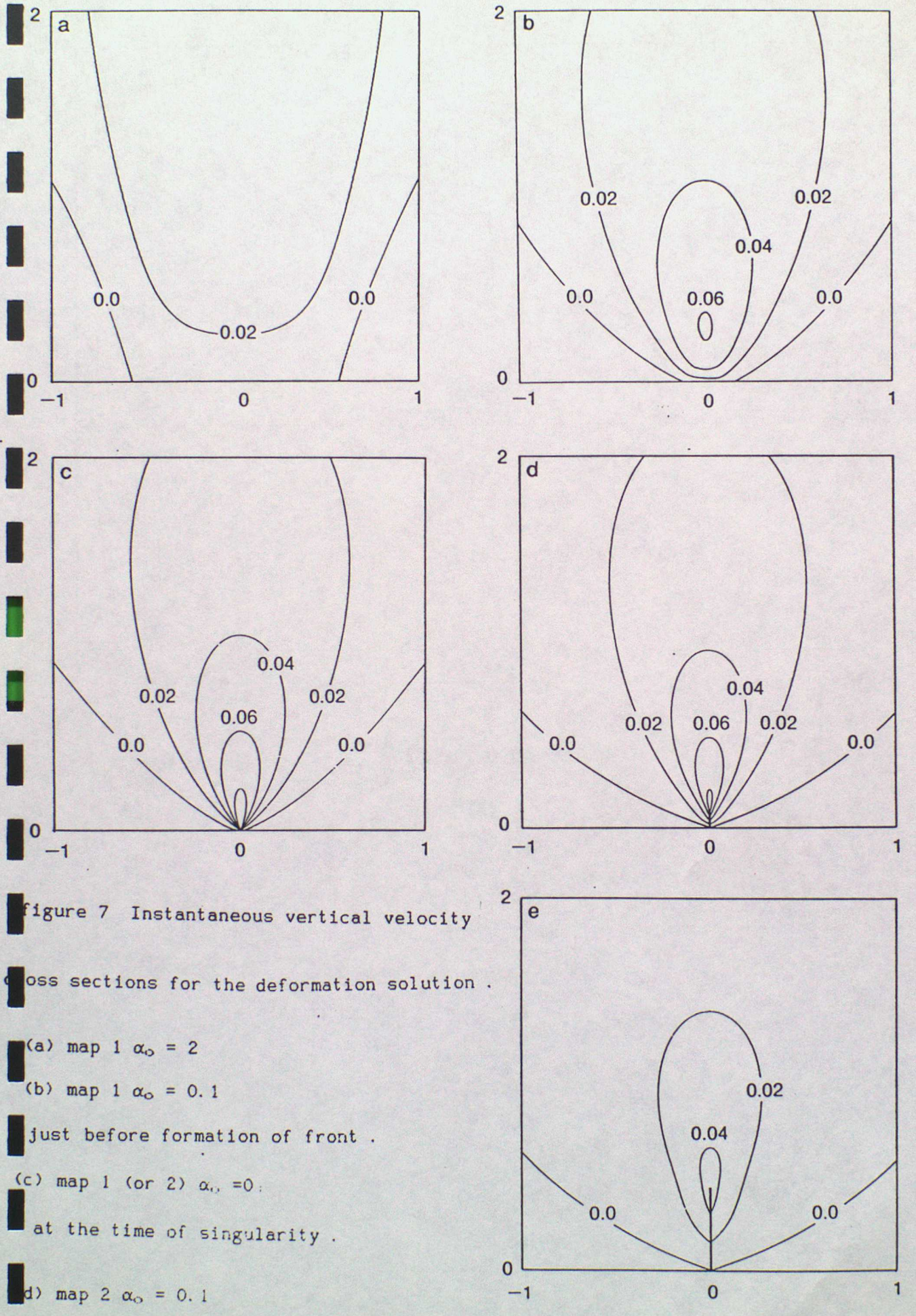

Figure 7 Instantaneous vertical velocity cross sections for the deformation solution.

(a) map 1 $\alpha_0 = 2$

(b) map 1 $\alpha_0 = 0.1$ just before formation of front.

(c) map 1 (or 2) $\alpha_0 = 0$ at the time of singularity.

(d) map 2 $\alpha_0 = 0.1$

(e) map 2 $\alpha_0 = 1$

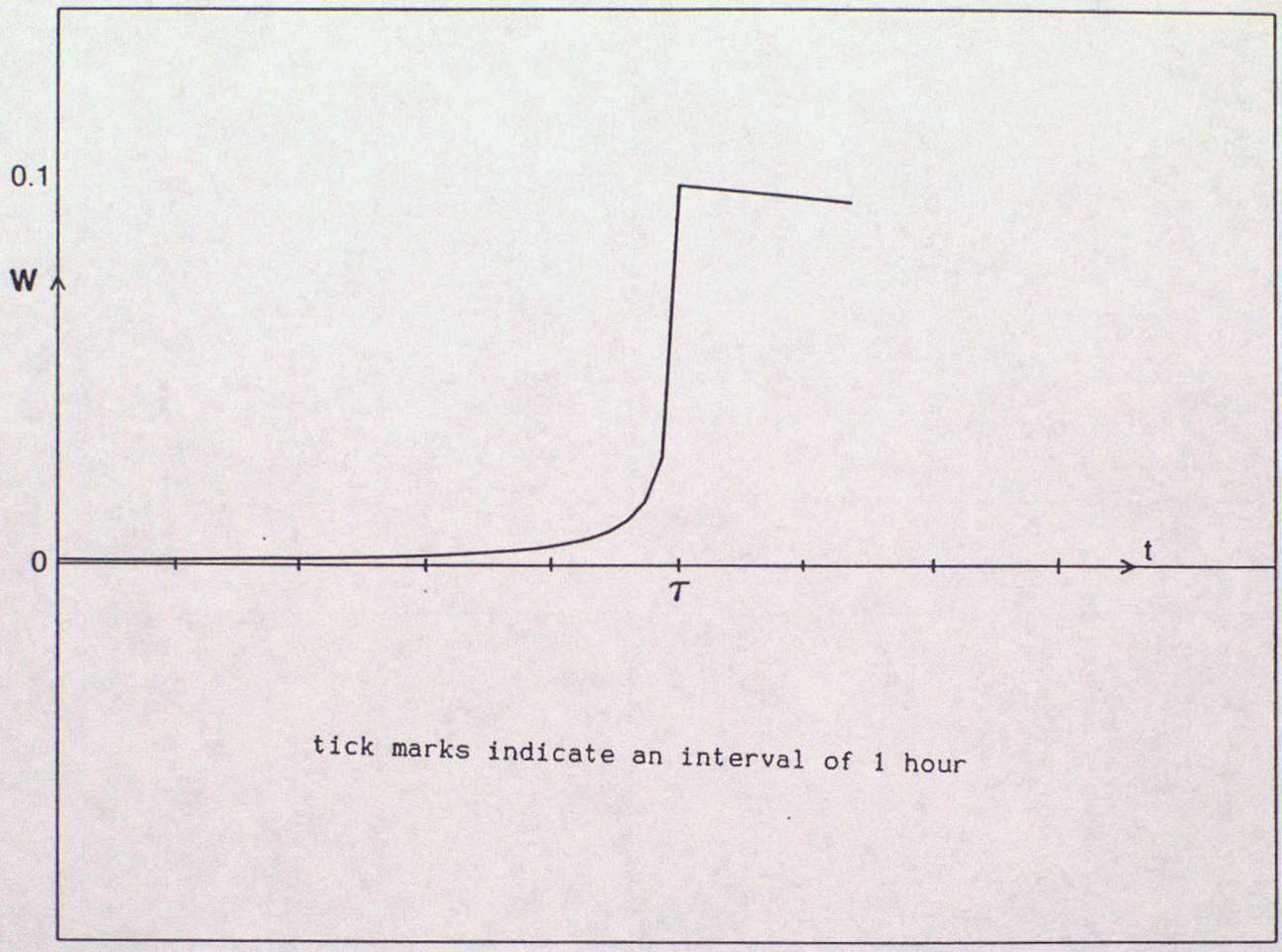

figure 8 Time series vertical velocity for an air parcel which arrives above the growing front .

figure 9 Cross-sections of ratio and rate of turn terms .

a) ratio at time τ -2½ hrs

b) ratio and c) turn terms at time τ .

d) ratio and e) turn immediately after time τ

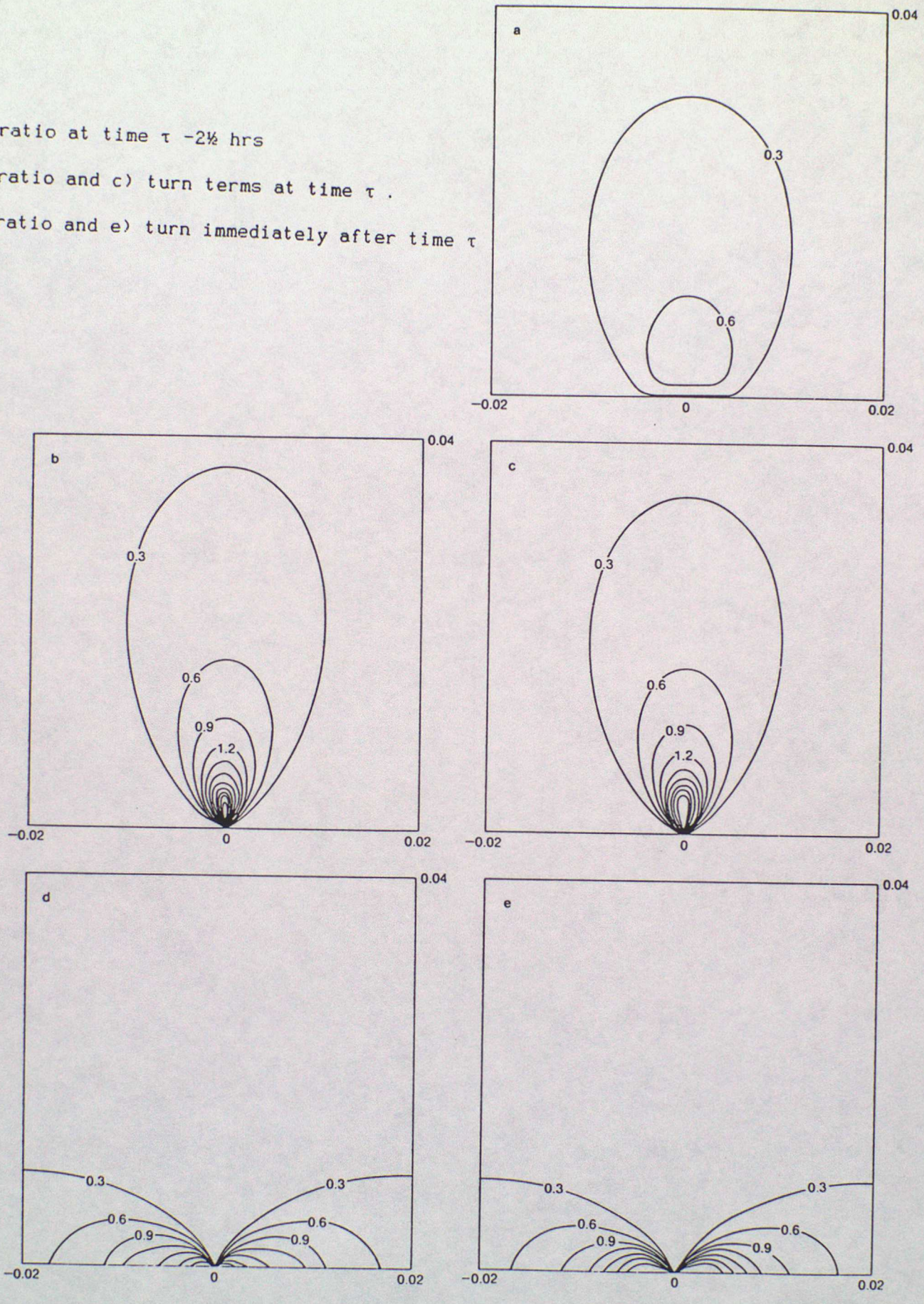

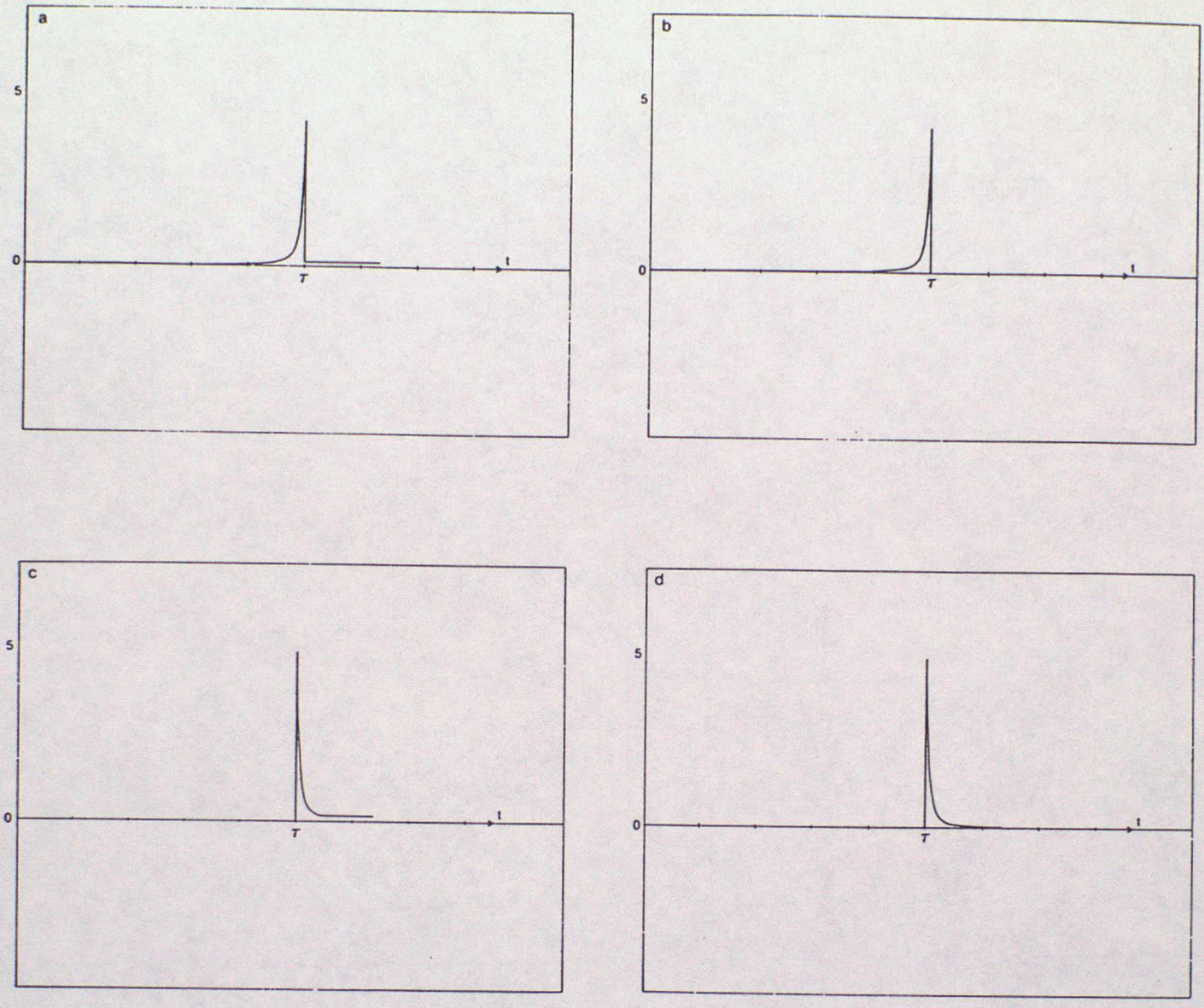

figure 10

Time series of the acceleration ratio (a) and (c), and the rate of turn terms ((b) and (d) .

(Above) for a parcel which finishes above the growing front.

(Below) for a parcel which is near the x-axis as the front forms .

tick marks indicate an interval of 1 hour

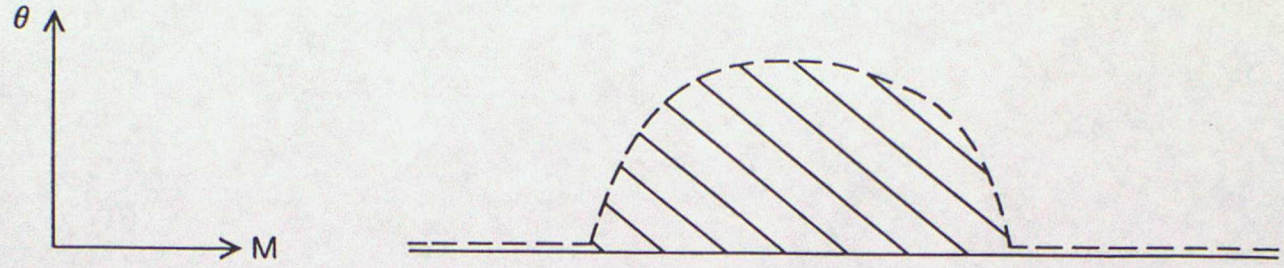

(a)

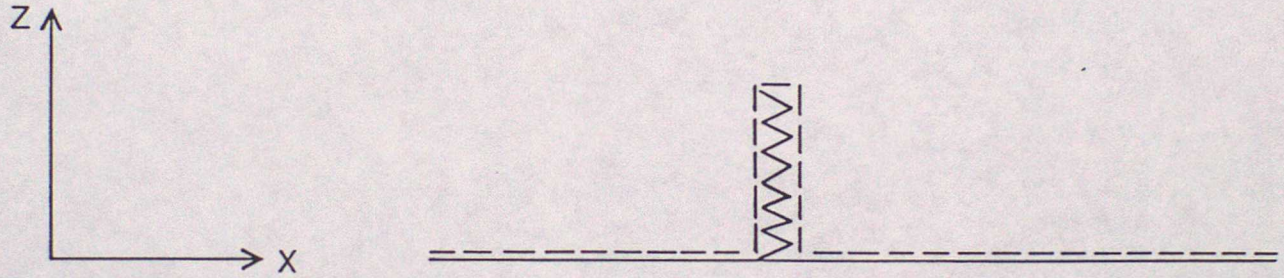

(b)

figure 11

Appendix 1. Algebraic limits of the map as α_o varies

The first mapping may be written as

$$Y = a \cosh[\sinh^{-1}(W\cosh(\alpha_o)) - \alpha_o] \qquad A.1$$

which on making use of the identity

$$\sinh^{-1}(x) = \ln[x + (x^2+1)^{1/2}] \qquad A.2$$

and expanding, we find that for $\alpha_o = 0$ may be written as

$$Y^2 = (W^2 + 1) \qquad A.3$$

To examine the limit as $\alpha_o \to \infty$ we may take the mapping in the form used by Gill(1981) :

$$Y = W + \exp(\alpha_o)\exp(-\zeta) \qquad A.4$$

writing c for $\cosh(\alpha_o)$ and using A.2 we obtain

$$Y = W + \exp(\alpha_o)/[Wc + c\,(W^2 + 1/c^2)^{1/2}] \qquad A.5$$

so that letting $\alpha_o \to \infty$ we obtain

$$Y \sim W + 1/W \qquad A.6$$

which is the discontinuity map of Shutts(1987).

Letting $\alpha_o \to -\infty$ in A.5 we find , as described above , that the limit is

$$Y = W \qquad \text{A.7 .}$$

The algebraic form of the third map is given by

$$Y = W + \exp(-\zeta)\ \sinh(\alpha_o) \qquad \text{A.8}$$

which, using the identity

$$\cosh^{-1}(x) = \ln\left[x + (x^2 - 1)^{1/2}\right] \qquad \text{A.9}$$

gives

$$Y = W \qquad \text{as } \alpha_o \to 0 \qquad \text{A.10}$$

$$Y = W + 1/2W \quad \text{as } \alpha_o \to \infty \qquad \text{A.11}$$

which is the algebraic form of the discontinuity map for a front of height 1/2.

Appendix 2. Expansion of the maps in parametric coordinates.

Mapping 1 : $a = 1 + \tanh(\alpha_o)$

$\alpha \geq \alpha_o \qquad 0 \leq \beta \leq \pi$

$$x = \sinh(\alpha)\cos(\beta) \,/\, \cosh(\alpha_o)$$

$$\theta = \cosh(\alpha)\sin(\beta) \,/\, \cosh(\alpha_o)$$

$$M = a \cosh(\alpha-\alpha_o) \cos(\beta)$$

$$Z = a \sinh(\alpha-\alpha_o) \sin(\beta)$$

Mapping 2 : $a = 1 + \tanh(\alpha_o)$

$\alpha \geq \alpha_o \qquad -\pi/2 \leq \beta \leq \pi/2$

$$x = \sinh(\alpha-\alpha_o)\sin(\beta)$$

$$\theta = \cosh(\alpha-\alpha_o)\cos(\beta)$$

$$M = \cosh(\alpha) \sin(\beta) \,/\, (a \cosh(\alpha_o))$$

$$Z = \sinh(\alpha) \cos(\beta) \,/\, (a \cosh(\alpha_o))$$

Mapping 3 : $a = 1 + \coth(\alpha_o)$

$\alpha \geq \alpha_o \qquad -\pi/2 \leq \beta \leq \pi/2$

$$x = \sinh(\alpha-\alpha_o) \sin(\beta)$$

$$\theta = \cosh(\alpha-\alpha_o) \cos(\beta)$$

$$M = \sinh(\alpha) \sin(\beta) \,/\, (a \sinh(\alpha_o))$$

$$Z = \cosh(\alpha) \cos(\beta) \,/\, (a \sinh(\alpha_o))$$

References

Cullen M J P 1983 Solutions to a model of a front forced by deformation . Quart J Roy Met Soc **109** 565 - 573

Cullen M J P and Purser R J 1984 An extended theory of semigeostrophic frontogenesis . J Atmos Sci **41** 1471-1497

Davies , H. C and Müller, J. C 1988 Detailed description of deformation induced semigeostrophic frontogenesis . Quart J Roy Met Soc **114** 1201 - 1220

Eliassen A 1983 The Charney-Stern theorem on barotropic-baroclinic instability. Pageoph. **121** 563-572

Gall R L Williams R T and Clark T L 1987 On the minimum scale of surface fronts . J Atmos Sci **44** 2562-2574

Gill A E 1981 Homogeneous intrusions in a rotating stratified fluid. J Fluid Mech **103** 275-295

Haynes P H and McIntyre M E 1987 On the evolution of vorticity and Potential vorticity in the presence of diabatic heating and friction or other forces . J Atmos Sci. **44** 828-841

Hoskins B J 1975 The geostrophic momentum approximation and the semigeostrophic equations . J Atmos Sci **32** 233-242

Hoskins B J 1982 The mathematical theory of frontogenesis Ann Rev Fluid Mech. 1982: 131-151

Hoskins B J and Bretherton F P 1972 Atmospheric frontogenesis models : mathematical formulation and solution . J Atmos Sci **29** 11 - 37

Keyser D and Anthes R A 1982 The influence of planetary boundary layer physics on frontal structure in the Hoskins-Bretherton horizontal shear model. J Atmos Sci **39** 1783-1802

Ou, H W 1984 Geostrophic adjustment: A mechanism for frontogenesis . J Phys Ocean **14** 984-1000

Purser R J and Cullen M J P 1987 A duality principle in semigeostrophic theory . J Atmos Sci **44** 3449 - 3468

Shutts G J 1987 Balanced flow states resulting from penetrative slantwise convection . J Atmos Sci **44** 3363 - 3376